The effects of turbulence on the flame structure and NO formation of ammonia turbulent premixed combustion at various equivalence ratios

Tingquan Tian[a], Chengbin Song[a], Haiou Wang[a,*], Chao Xu[b], Kun Luo[a], Jianren Fan[a]

[a] *State Key Laboratory of Clean Energy Utilization, Zhejiang University, Hangzhou 310027, PR China*
[b] *Energy Systems Division, Argonne National Laboratory, Lemont, IL 60439, USA*

Abstract

Ammonia is carbon-free and is regarded as a potential fuel to address global warming issues. In this work, three-dimensional direct numerical simulations (DNS) of ammonia/air turbulent premixed flames were performed to explore the influence of turbulence and equivalence ratio on the flame structure and NO formation characteristics. Two equivalence ratios were considered, *i.e.* $\phi = 0.9$ and $\phi = 1.1$. The general flame structures were presented and species distributions were examined. The NO mass fraction was found to be the highest in the product for the lean case and in the reaction zone for the rich case. The conditional mean values of species mass fractions and reaction rates were compared with those of the unstrained and strained laminar premixed flames to explore how well the laminar flame structures can approach those of the turbulent flame. The budget analysis of the species transport equations showed that turbulent diffusion plays an important role in species transport. The turbulent diffusivity D_T was estimated using the gradient hypothesis based on the DNS data. Various laminar flame simulations with different diffusivities were carried out. It was shown that the conditional means of the DNS agree well with those of the laminar flames including D_T in the transport property calculation. The global

*Corresponding author: Haiou Wang
Email address: wanghaiou@zju.edu.cn (Haiou Wang)

and local NO formation characteristics were investigated. It was found that the mean NO production conditioned on the progress variable is lower compared with the corresponding laminar flame in the rich case. However, the relative contributions from various NO pathways are rarely affected by turbulence. The NO mass fraction is higher in negative curvature regions compared with positive curvature regions of the flame surface for the rich case, which is due to the preferential diffusion of H_2 and other radicals and the enhanced NO pathways in negatively curved regions.

Keywords: Turbulent ammonia flames, Flame structure, NO_x emission, Direct numerical simulation

1. Introduction

Traditional fossil fuels, such as coal, petroleum and natural gas, have been widely used in power generation, transportation and industry sectors. During the process of fossil fuel combustion, the greenhouse gas (GHG) emission is a major issue that threatens the development and safety of human society. To reduce the GHG emission, hydrogen may be a potential clean fuel, of which the products are water and a certain level of NO_x. However, many important unsolved challenges in transportation and storage hinder the wide utilization of hydrogen [1]. Ammonia is regarded as a promising alternative to hydrogen for its well-established industry of production, storage, transport and utilization. As a carbon-neutral fuel, the main problems for ammonia combustion include the low reactivity and NH_3/NO emission. Therefore, the effective combustion of ammonia and the control of pollutant emission have attracted extensive attention.

Recently, turbulent ammonia combustion has been investigated experimentally using advanced laser diagnostics [2–12]. Brackmann *et al.* [2] used laser-induced fluorescence (LIF) for NH in premixed NH_3/air flames. Thinning and

broadening of the NH layer were observed, which indicated the coupling of turbulence and chemical reactions. Weng *et al.* [4] proposed the laser-induced photofragmentation fluorescence (LIPF) for quantitative ammonia imaging in combustion environments. Fan *et al.* [8] studied the flame surface density, flame-surface area ratio, and turbulent burning velocity of premixed ammonia/air jet flames with various Karlovitz numbers (Ka). Fan *et al.* [9] also investigated instantaneous structures of turbulent premixed ammonia/air jet flames on a piloted jet burner, and it was found that the NH layer becomes progressively thickened and distorted by turbulence with increasing turbulent intensity and axial distance.

Numerical simulations [13–21] have also been performed to provide useful information of turbulent ammonia flames. Wei et al. [13] investigated the flame topology and the blow-off characteristics of an ammonia flame in a model gas turbine combustor using large eddy simulation (LES). Okafor *et al.* [14] performed LES of a micro gas turbine swirl combustor, and examined the flow field, flame structure and emission characteristics. Somarathne *et al.* [15] explored the effects of pressure on NO, unburnt NH_3 and H_2 in a gas turbine like combustor using LES. It was found that emissions of NO and unburnt NH_3 both decrease with increasing pressure. Direct numerical simulation (DNS) is considered as a powerful tool to investigate the underlying physics in turbulent flames, from which fundamental understanding of turbulent ammonia flames can be obtained [19–25]. Netzer *et al.* [19] performed two-dimensional DNS of $NH_3/H_2/N_2$/air premixed flames with various equivalence ratios, and investigated the curvature effects on NO formation. It was found that the thermo-diffusive effects affect the local equivalence ratio, which further influence the NO formation. Rieth *et al.* [20] examined the effects of the diffusion of H_2 and H on hydrogen/ammonia/air flames. Yang *et al.* [21] reported the influences of hydrogen addition on ammo-

nia combustion, and found that the reactivity of the flame and the combustion process are enhanced. Despite of these studies, there is a lacking of DNS of pure ammonia/air premixed flames.

Many studies have revealed the effects of turbulence on the flame structure of hydrocarbon fuels. Turbulent flames are subjected to turbulent straining, and the response of the flame structure to tangential strain rate has been widely investigated [26–32]. It was found that flame structures in weak turbulence are similar to those of unstrained flames. As turbulent straining increases, the flame structures are largely affected by turbulence. Hawkes et al. [31] found that the results from strained reactants-to-products laminar flames show good agreements with the turbulent flame results in the thin reaction zones regime. Wang et al. [22] evaluated the effects of strain rate on the structure of high Ka flames and found that steady strained laminar flames can still represent certain aspects of the mean turbulent flame structure in the broken reaction zones regime when the strain rate of the mean flow is employed.

An important effect of turbulence is to modify the flame structure through turbulent mixing [33–35], which would enhance diffusion of radicals and heat. As a first approximation, the effect of turbulent mixing on flame structure could be assessed by increasing the species and thermal diffusivity in laminar flame simulations. The unsteady behavior of turbulent flames could also be potentially revealed by varying the diffusivity of laminar flames. In previous studies, certain aspects of the response of mean flame structure to intense turbulence have been reproduced by laminar flame simulations with enhanced diffusivity [20, 36, 37]. Savard *et al.* [38] investigated the differential diffusion in C_7H_{16}/air premixed turbulent flames using DNS. The result showed that turbulence affects the flame structure by increasing effective species and thermal diffusivities. Aspden et al. [39] reported turbulent premixed flames with large Ka, where the species

reached a state that is different from that in both non-unity and unity Le laminar flames. The effects of diffusivity on ammonia flames, however, have not been reported before in the literature.

NO emission is a critical issue in the application of ammonia combustion [40–46]. The interactions of turbulence and chemistry play an important role in the NO formation process. There are a number of studies which explored the effects of turbulence on the NO formation of hydrocarbon [47–49] and hydrogen [50, 51] flames. Trisjono and Pitsch [49] performed DNS of a lean premixed methane/air jet flame and various NO pathways were analyzed. The NO pathways were found to be affected by mean shear layer and turbulence. Day et al. [50] observed an increase in NO emission in turbulent hydrogen lean premixed flames relative to their laminar counterpart due to the cellular flame structures. Similar observations were made in a lean premixed hydrogen low swirling flame [51]. However, existing knowledge about the mechanisms of turbulence and NO chemistry interactions in turbulent ammonia/air flames is insufficient.

In this context, the present work focuses on the effects of turbulence and equivalence ratio on the ammonia flame structure and NO formation. The objectives are as follows. First, three-dimensional DNS of ammonia/air turbulent premixed flames are performed with varying equivalence ratio, and the general characteristics of the flames are presented. Second, the effects of the turbulence on the flame structure are investigated by the analysis of the transport equation of the species. Third, the turbulent diffusivity is estimated from the DNS data and laminar premixed flames with various species/thermal diffusivities are simulated to understand the influence of transport models on the flame structures. Finally, the effects of turbulence and equivalence ratio on the formation of NO are studied via the chemical pathway analysis. The global and local effects of turbulence on the formation of NO are also explored, and the related

phenomenon of preferential diffusion is discussed.

2. Computational details

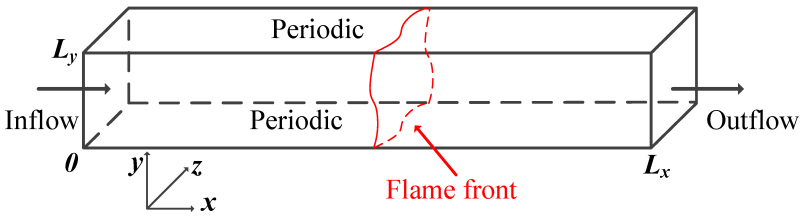

Figure 1: Schematic of the DNS configuration.

In this section, the computational details of the DNS, including the DNS configuration, the reaction mechanism and the numerical methods, are described. The configuration of a freely propagating turbulent flame is considered. A schematic diagram of the configuration is showed in Fig. 1. The reactant consists of ammonia/air mixture with a temperature of 300 K. The pressure is 1 atm. Fig. 2a shows the flame thickness and the flame speed of laminar premixed NH_3/air flames at 1 atm and 300 K calculated using the same mechanism as the DNS, which is reduced from the Mathieu mechanism [52] as will be described in detail later. It is seen that the flame speed first increases and then decreases with increasing equivalence ratio, while the flame thickness first decreases and then increases with increasing equivalence ratio. The maximum flame speed and the minimum flame thickness is achieved at around $\phi = 1.1$. Fig. 2b shows the mass fractions of NO_2, NO, NH_3, and H_2 in the product side (sampled at 4 cm downstream of the location of maximum heat release rate) at various ϕ. It is seen that the mass fraction of NO first increases and then decreases with increasing equivalence ratio, and the maximum NO mass fraction is achieved around $\phi = 0.9$, while the mass fraction of NH_3 increases monotonically with increasing equivalence ratio. The total emission of NO and NH_3 is minimum

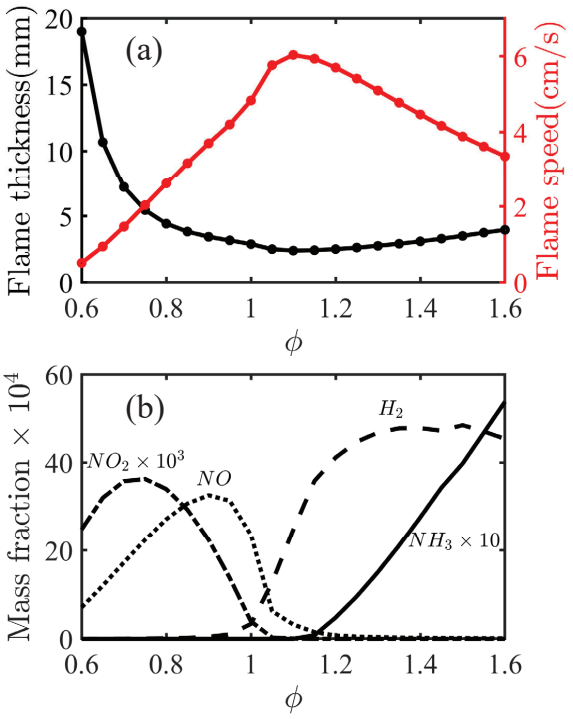

Figure 2: (a) The flame thickness and the flame speed of NH_3/air flames at 1 atm and 300 K. (b) Mass fractions of NO_2, NO, NH_3, and H_2 at 4 cm downstream of the maximum heat release rate location at various ϕ.

around $\phi = 1.1$, as also reported in our previous work [53]. Thus, two equivalence ratios, *i.e.* $\phi = 0.9$ and $\phi = 1.1$, were considered in the present DNS study to explore the influence of equivalence ratio on the emission characteristics. Under these conditions, the corresponding laminar flame speed S_L is 0.037 (0.061) m/s, the laminar flame thickness δ_L is 3.46 (2.40) mm, and the laminar flame time τ_L is 93.51 (39.34) ms for the lean (rich) case. The inflow velocity is chosen to match the corresponding turbulent flame velocity, so that the whole flame structure maintains statistically stationary at a fixed location of the computational domain.

The simulations were initialized with a corresponding laminar premixed flame solution. Homogeneous isotropic turbulence based on a Passot-Pouquet

kinetic energy spectrum [54] is used as the initial turbulence field. The turbulence parameters are illustrated in Table 1, where u' is the turbulent velocity, l_t is the turbulent integral length scale, and τ_e is the eddy turn-over time. The turbulent Reynolds number is defined as $Re_t = u'l_t/\nu$, where ν is the kinematic viscosity. The Karlovitz number (Ka) is defined as $Ka = \tau_L/\tau_\eta$, where $\tau_\eta = (\nu l_t/u'^3)^{1/2}$ is the Kolmogorov time scale. u' and l_t are selected to keep Re_t and Ka the same for the lean and rich case. It is obvious that the Ka of the DNS is high and the flame is in the broken reaction zones regime of the combustion regime diagram. A linear forcing method [54] was applied to maintain a statistically steady turbulence field, which has been widely used for understanding turbulence/flame interactions [55, 56]. The linear forcing method injects energy into different scales of the flow, and it generates very similar vorticity dynamics compared to those in laboratory-scale flames [57] and DNS flames with shear layer turbulence [23]. To prevent the influence of forcing on the inflow/outflow physical boundaries, the forcing was turned off near the inlet and outlet.

Table 1: Simulation parameters

ϕ	u' (m/s)	l_t (mm)	τ_e (ms)	Re_t	Ka
0.9	0.767	3.09	4.03	157	287
1.1	1.18	2.00	1.69	157	287

A skeletal mechanism of ammonia/air combustion, including 20 species and 113 elementary reactions, is developed for the DNS study, which is reduced from the Mathieu mechanism [52]. The Mathieu mechanism consists of 55 species and 275 elementary reactions, and it has been validated extensively in previous literature [53, 58] with promising performance in predicting the auto-ignition delay time and the laminar flame propagating velocity. To systematically reduce the size of the chemical mechanism, mechanism reduction based on directed relation graph (DRG) [59] and sensitivity analysis is performed as part of this study. A large set of reaction states are sampled for mixture of the NH_3/H_2

blend and air over the parameter range of H_2 blending ratio from 0 to 1, pressure from 1 to 30 atm, equivalence ratio from 0.5 to 1.5, inlet temperature of 300 K for perfectly stirred reactors (PSRs), and initial temperature from 1000 to 1600 K for auto-ignition. An error tolerance of 0.1 (*i.e.* worst case error of 10%) is used in both DRG and sensitivity analysis. The comparisons of the results from the current mechanism and the Mathieu mechanism are provided in the Supplementary Material. Constant and non-unity species Lewis numbers (Le), determined from a fit to mixture-averaged transport properties in a premixed flame, were employed to provide species diffusivities. The resultant species Le are also provided in the Supplementary Material.

The computational domain is $L_x \times L_y \times L_z = 10.57 \times 1.76 \times 1.76$ cm^3 in the lean case, and is $L_x \times L_y \times L_z = 6.85 \times 1.14 \times 1.14$ cm^3 in the rich case. Note that the flame thickness of the lean case is larger than that of the rich case, so that the computation domain of the two DNS cases is different. Improved Navier–Stokes characteristic boundary conditions (NSCBC) [60] were used to prescribe the boundary conditions. Specifically, non-reflecting inflow/outflow boundaries are used at inlet ($x = 0$) and outlet ($x = L_x$), while the lateral boundary conditions are periodic. In the DNS, the Kolmogorov length scale η_k is estimated to be 69 (49) μm for the lean (rich) case. A uniform grid of $\Delta x =$ 104.7 (67.9) μm is used for the lean (rich) case. The grid resolution is chosen to adequately resolve both the flame and turbulence. The resultant number of grids is $N_x \times N_y \times N_z = 1008 \times 168 \times 168$ for both cases.

The simulation was performed using the DNS code 'S3D' [61]. The DNS code has been used widely in studies of turbulent flames [22, 23, 62, 63]. The code solves the compressible governing equations of mass, momentum, total energy and mass fractions of chemical species including chemical reactions using a fourth-order Runge-Kutta method for time advancing and an eighth-order

finite differencing spatial scheme. A tenth-order filter is employed to remove high-wave number oscillations [64].

The simulations were performed at the National Supercomputer Center in Beijing, China. The simulations required about 1.0 million CPU hours on 1800 cores (on AMD EPYC 7452 processors).

3. Results and discussion

In this section, the general characteristics of the turbulent premixed flames are first presented. Then, the effects of turbulence on the flame structure are investigated by analyzing species transport equations. Following that, turbulent mixing of various cases is quantified and the turbulent diffusivity is determined. A simple model of one-dimensional laminar flames is employed to account for the effects of turbulent mixing, and its performance is evaluated by comparing the species distributions between the laminar and DNS flames. Finally, the NO formation characteristics are examined via NO pathways both locally and globally. The effects of turbulence and equivalence ratio on the formation of NO are also evaluated.

3.1. General characteristics

Figure 3 shows the evolution of the normalized S_T for both cases. The turbulent flame speed is defined as the fuel reaction rate integrated over the domain divided by the product of the cross-sectional area and the fuel mass fraction:

$$S_T(t) = -\frac{1}{\rho_u(\mathrm{Y}_{\mathrm{NH_3,u}} - \mathrm{Y}_{\mathrm{NH_3,b}})L_yL_z}\int_V \dot{\omega}_{\mathrm{NH_3}}(x,y,z,t)dV \tag{1}$$

where $\dot{\omega}_{\mathrm{NH_3}}$ is the reaction rate of $\mathrm{NH_3}$, and V denotes the computational domain. The subscripts 'u' and 'b' imply quantities in the unburnt and burnt gas,

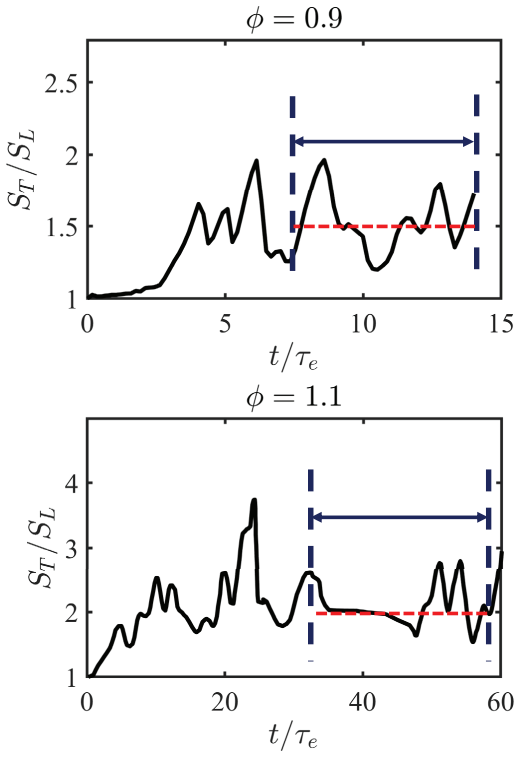

Figure 3: The evolution of the normalized turbulent flame speed. The red dashed lines represent the mean values of the turbulent flame speed.

respectively. The same definition of turbulent flame speed has been widely used in previous studies of turbulent premixed flames [37, 65–70]. As can be seen, S_T varies with time for both lean and rich cases due to the unsteady behavior of turbulent flames. Nevertheless, the flames reach a statistically steady state after the initial period. The statistics presented in the following are averaged within a range of time during this stage, which is marked by the black dash lines in Fig. 3. The mean value of S_T is $1.48S_L$ and $1.8S_L$ for the lean and rich case (as marked by the red dash lines in Fig. 3), respectively, indicating that turbulence improves the turbulent flame speed more significantly in the rich case than in the lean case.

Figure 4 shows the contours of $Y_{\mathrm{NH_3}}$, Y_{NO}, $Y_{\mathrm{H_2}}$, vorticity magnitude and heat

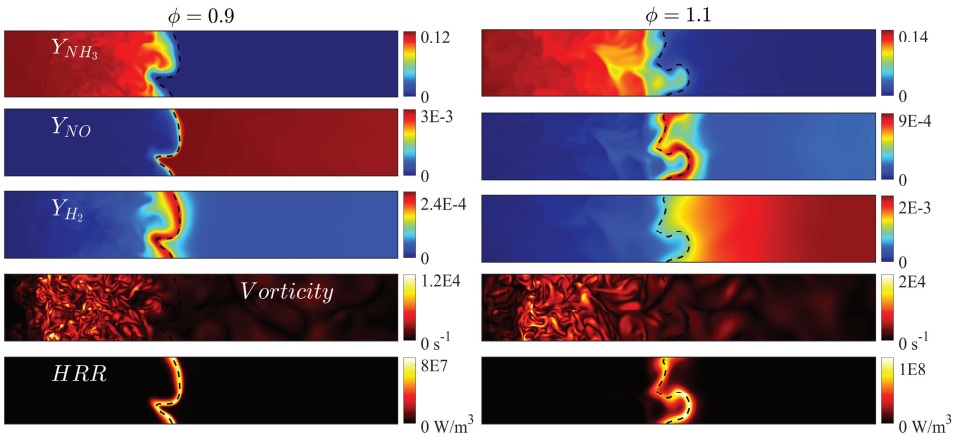

Figure 4: Contours of NH_3, NO and H_2 mass fractions, vorticity magnitude and heat release rate (HRR) in a typical $x-y$ plane of the lean and rich cases. The black dashed lines represent the flame front.

release rate (HRR) in a typical $x-y$ plane. Note that the peak HRR corresponds to the iso-line of $c = 0.96$ and 0.82 for the lean and rich case respectively, which is used to denote the flame front in the present work. The progress variable c is defined as $c = (Y_{\mathrm{NH_3}} - Y^u_{\mathrm{NH_3}})/(Y^b_{\mathrm{NH_3}} - Y^u_{\mathrm{NH_3}})$. It is seen that $Y_{\mathrm{NH_3}}$ decreases from the reactant to product, and the ammonia concentration in the product is negligible. Note that in the lean case NH_3 is consumed completely, while in the rich case the excess NH_3 is pyrolyzed to H_2, as shown in the contour of $Y_{\mathrm{H_2}}$. NO is the most important pollutant of ammonia combustion and its mass fraction is the highest in the product for the lean case, while it is the highest in the reaction zone for the rich case. The species H_2 is concentrated in the reaction zone for the lean case while it is significant in the product for the rich case due to the pyrolization of NH_3. The different distributions of the species mass fractions indicate that the flame structure is significantly influenced by equivalence ratio. It can be seen that the magnitude of vorticity is reduced in the streamwise direction, due to the fact that the kinematic viscosity increases as reaction progresses. It is also observed that the values of Y_{NO} and HRR are

higher on the flame front with negative curvature rather than positive curvature in the rich case, which will be discussed in detail in Sec. 3.3. Here, curvature is calculated as $\nabla \cdot \mathbf{n}$, where $\mathbf{n}$ is the normal vector of the flame front, *i.e.* $\mathbf{n} = -\nabla c/|\nabla c|$. According to the definition, $\mathbf{n}$ points towards the reactant. Curvature is positive when the center of curvature is in the product side of the flame, while it is negative when the center is in the reactant side. Although not shown, the observed trends of the contours are very similar between different time instants after the flames reaching statistically stationary.

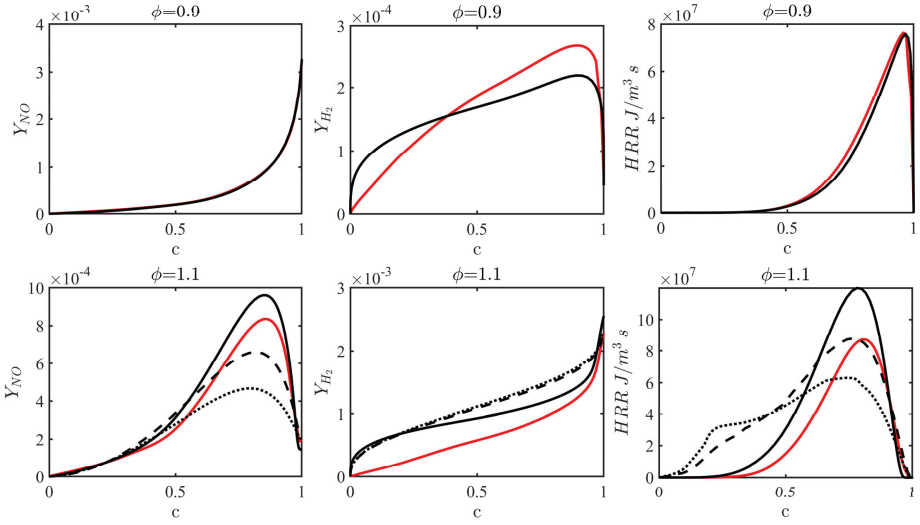

Figure 5: Comparation between the conditional means of the DNS and the laminar flame profiles for Y_{NO}, $Y_{\mathrm{H_2}}$ and HRR in c space. The red and black solid lines denote the DNS results and the unsrained laminar flame profiles, respectively. Strained laminar flames are calculated for the rich case: '- - -' : $S = 2128\ s^{-1}$; '...' : $S = 4256\ s^{-1}$.

In flamelet modelling approach of turbulent combustion [71], turbulent flames are considered to be a collection of stretched laminar flames, *i.e.* flamelets, which are subjected to the tangential strain rate caused by turbulence [26–30]. To understand how well the structures of the laminar flame can approach those of the turbulent flame, Fig. 5 shows the conditional means of Y_{NO}, $Y_{\mathrm{H_2}}$ and HRR in c space from the DNS and the profiles from various laminar flames.

The conditional means of the DNS are further averaged in time after the flames reaching statistically steady state. It is noted that, for the lean case, the profiles of Y_{NO} and HRR are similar between the DNS and the unstrained laminar flame, indicating the turbulent flame structure is largely uninfluenced by turbulence in c space. In contrast, there is evident difference between the structures of the turbulent flame and those of the unstrained laminar flame for the rich case. Therefore, strained laminar flames are calculated for this case. A reactant-to-product counterflow configuration, following previous studies [31], is chosen for the strained laminar flame calculations. The temperature and composition in the reactant and product sides of the counterflow configuration are kept the same as those of the unstrained laminar flames. Two values of strain rates are implemented for the laminar flames of the rich case, *i.e.* $\mathrm{S} = 2128\ \mathrm{s}^{-1}$ and 4256 s^{-1}. It is worth noting that the peak HRR of the strained laminar flame for the rich case with $\mathrm{S} = 2128\ \mathrm{s}^{-1}$ matches that of the conditional mean HRR of the turbulent flame. As can be seen, the peak HRR of the laminar flames decreases with increasing strain rate. A similar trend is observed for the profiles of Y_{NO}. As for $Y_{\mathrm{H_2}}$, the predictions from laminar flames are always higher than that from the DNS, and the profiles almost overlap for the two strained laminar flames.

3.2. Effects of turbulence on the flame structure

3.2.1. Budget analysis

The species distributions are largely affected by turbulence. To further understand the species distribution characteristics, the budget of species transport equation in the context of Reynolds-averaged Navier-Stokes simulation (RANS)

is analyzed, which can be written as [72]:

$$\frac{\partial \overline{\rho}\widetilde{Y_k}}{\partial t} = \underbrace{\overline{\dot{\omega}_k}}_{T_1} \underbrace{- \frac{\partial \overline{\rho}\widetilde{u}_i\widetilde{Y_k}}{\partial x_i}}_{T_2} \underbrace{- \frac{\partial \overline{\rho V_{k,i} Y_k}}{\partial x_i}}_{T_3} \underbrace{- \frac{\partial \overline{\rho} \widetilde{u_i'' Y_k''}}{\partial x_i}}_{T_4} \tag{2}$$

where the overbar denotes the Reynolds averaging operation and the tilde denotes the Favre averaging operation as $\widetilde{\psi} = \overline{\rho\psi}/\overline{\rho}$. The terms on the RHS of the equation represent the reaction term (T_1), the convection term (T_2), the molecular diffusion term (T_3) and the turbulent diffusion term (T_4).

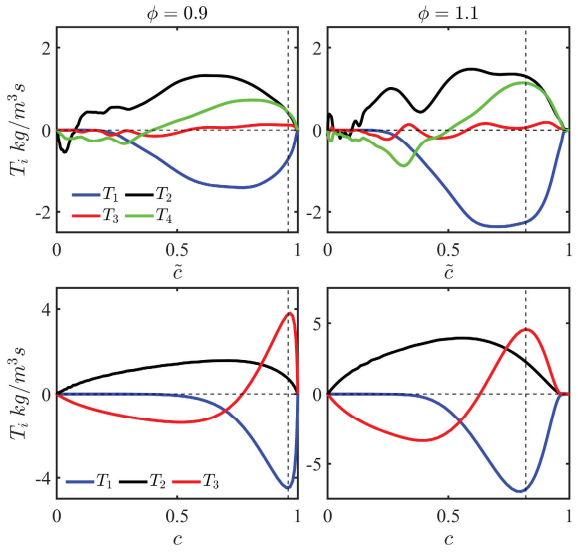

Figure 6: The NH_3 transport equation budget as a function of $\tilde{c}/c$ for turbulent (top) / laminar (bottom) flames. The vertical dashed line indicates the (mean) flame front.

Figures 6-8 show the budget of species transport equations for NH_3, NO and H_2 of the turbulent flames and the corresponding unstrained laminar flames. In the laminar flame, the turbulent diffusion term is absent. It is first observed that the magnitudes of the budget terms in the turbulent flames are lower than those in the laminar flames. Note that the thickness of the turbulent flame brush is much larger than the laminar flame thickness. The budget terms are averaged

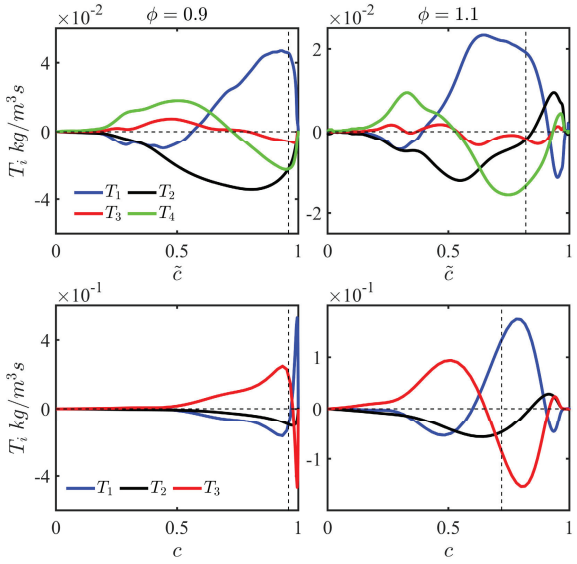

Figure 7: The NO transport equation budget as a function of $\tilde{c}/c$ for turbulent (top) / laminar (bottom) flames. The vertical dashed line indicates the (mean) flame front.

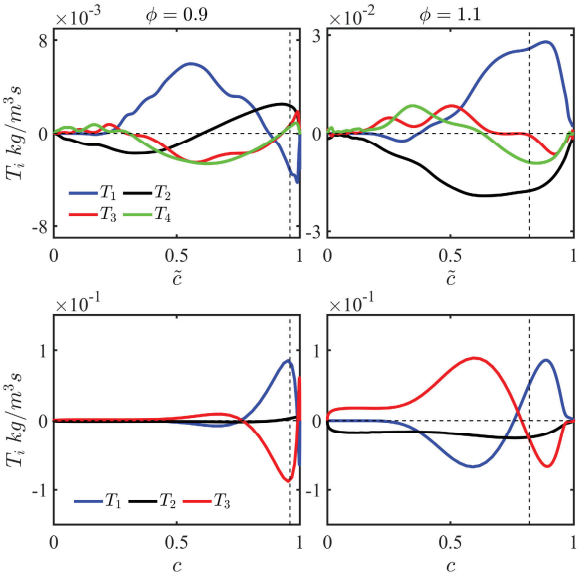

Figure 8: The H_2 transport equation budget as a function of $\tilde{c}/c$ for turbulent (top) / laminar (bottom) flames. The vertical dashed line indicates the (mean) flame front.

in a thicker flame brush, which results in lower values compared to those of the laminar flames. For the budget terms of Y_{NH_3}, reaction is small close to the fresh gas, and convection is balanced by molecular diffusion and turbulent diffusion in the turbulent flames, and is balanced by molecular diffusion in the laminar flames. As $\tilde{c}$ or c increases, reaction is dominant and is balanced by convection and turbulent diffusion in the turbulent flames, and is balanced by molecular diffusion in the laminar flames. The difference of the budget terms between the lean case and rich case is not obvious. The profiles of the budget terms for NO are more complex. It is seen that NO is produced in large $\tilde{c}$ or c regions and is consumed in the preheat zone for the lean case. In contrast, NO is consumed in small/large $\tilde{c}$ or c regions and is produced elsewhere for the rich case. This trend explains the distribution of NO in Fig. 4, *i.e.* the mass fraction of NO is the highest in the product in the lean case, while it peaks in the reaction zone in the rich case. The species H_2 is an important radical in ammonia combustion. Fig. 8 shows that H_2 is produced in the reaction zone and is consumed as $\tilde{c}$ or c increases in the lean case, while in the rich case it is produced both in the reaction zone and in the product. The increase of Y_{H_2} in the product of the rich case is due to the pyrolization of the excess NH_3.

3.2.2. Turbulent diffusivity

The above analysis suggests that turbulent mixing plays an important role in species transport in physical space. Turbulent mixing can be characterized by the turbulent flux $\widetilde{u_i''\psi''}$ of the scalar ψ. In RANS, $\widetilde{u_i''\psi''}$ is usually modeled using the gradient hypothesis: [73]:

$$\widetilde{u_i''\psi''} = -D_T \frac{\partial \widetilde{\psi}}{\partial x_i} \tag{3}$$

where D_T is the turbulent diffusivity to be determined. In the DNS, the turbulent scalar flux $\widetilde{u_i''\psi''}$ and the gradient of the Favre averaged scalar $\partial\widetilde{\psi}/\partial x_i$ can be calculated and the turbulent diffusivity could be estimated. As the mean flame propagates in the streamwise direction, only the streamwise component of the turbulent scalar flux $\widetilde{u''\psi''}$ is discussed in the following.

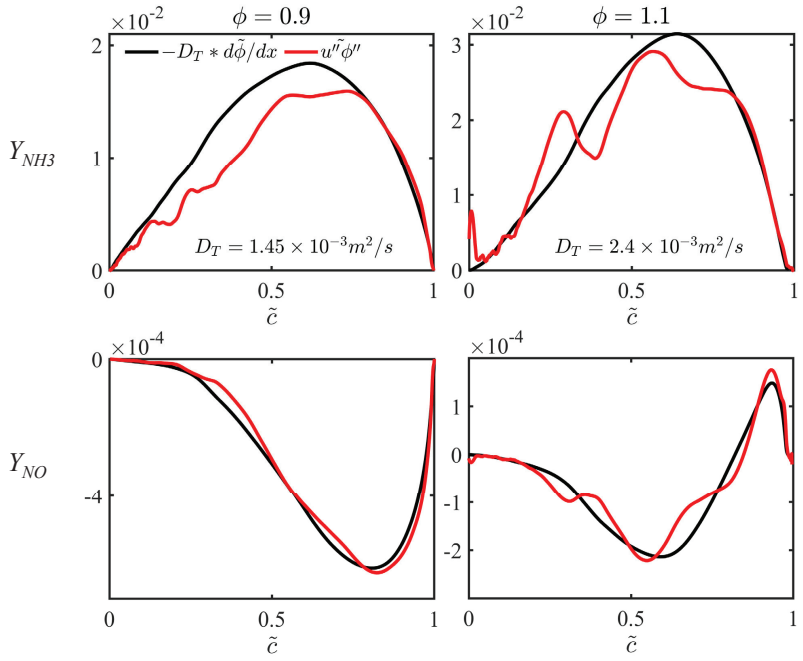

Figure 9: The actual and modeled turbulent scalar flux for NH_3 (top) and NO (bottom).

Figure 9 shows the turbulent scalar flux $\widetilde{u''\psi''}$ as a function of the Favre averaged progress variable $\tilde{c}$ based on two scalars, *i.e.* Y_{NH3} and Y_{NO}. The modeled turbulent flux using $-D_T\partial\widetilde{\psi}/\partial x$ is also plotted with a best fit D_T, the value of which is 1.45 $\times 10^{-3}$ and 2.4 $\times 10^{-3}$ m^2/s for the lean and rich case, respectively. It can be seen that the actual and modeled turbulent fluxes agree very well. Note that the values of D_T are of the same order as $l_t u' = 2.36 \times 10^{-3}$ m^2/s, which has been commonly used for evaluating D_T in RANS [74].

Turbulence essentially increases the species and heat mixing at the same rate.

The intensity of turbulent mixing can be measured by turbulent diffusivity D_T as described above. By assuming the same turbulent diffusivity could be applied to all scalars, a simple model is employed to account for the effects of turbulent mixing with one-dimensional laminar flame simulations. The effective species diffusivity $D_{k,eff}$ and the effective thermal diffusivity $D_{th,eff}$ of the laminar flames are written as:

$$D_{k,eff} = D_{k,0} + D_T \tag{4}$$

$$D_{th,eff} = D_{th,0} + D_T \tag{5}$$

where the subscript '0' denotes the laminar flame value. The effective Lewis number, $Le_{k,eff}$, is computed as:

$$Le_{k,eff} = \frac{D_{th,eff}}{D_{k,eff}} = \frac{D_{th,0} + D_T}{D_{k,0} + D_T} \tag{6}$$

It is obvious from Eq. 6 that the large values of D_T result in a unity effective species Le.

The structures of the turbulent flames and various laminar flames are compared in the following. Fig. 10 shows the conditional means of Y_{NO}, $Y_{\mathrm{H_2}}$ and Y_{HNO} and the laminar flame profiles with D_T included in the transport property calculation. The profiles from laminar flames with non-unity and unity Le are also shown for comparison. It is seen that there are large fluctuations of the species mass fractions in the progress variable space, as expected in the current high Ka flames. The conditional means of the turbulent flame are very different from the profiles of the laminar flame with non-unity Le for these species. In contrast, the profiles of the laminar flame with D_T included in the transport property calculation correspond to those of the turbulent flame well. This is particularly true for the profiles of Y_{NO} and $Y_{\mathrm{H_2}}$. Therefore, one of the influences of turbulence on flame structure is to increase the thermal and species diffusion,

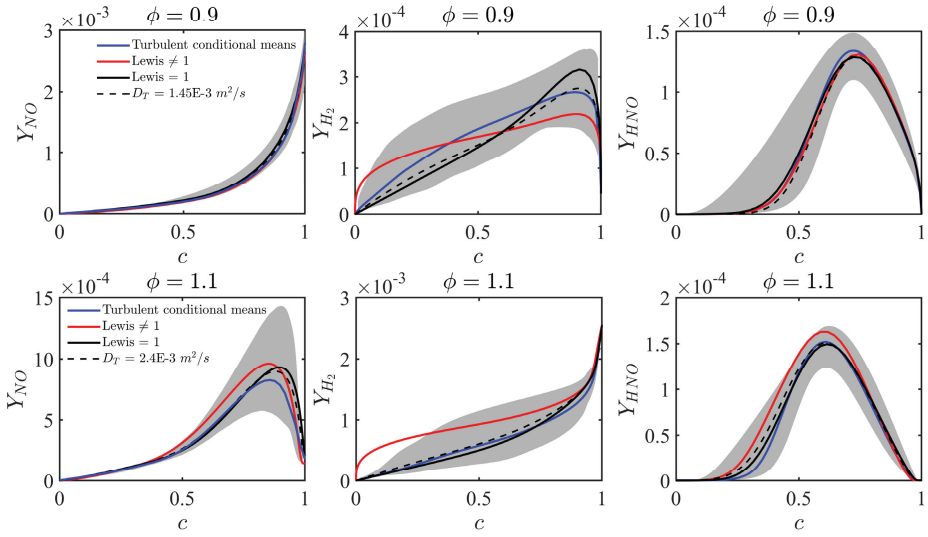

Figure 10: The conditional means of Y_{NO}, $Y_{\mathrm{H_2}}$ and Y_{HNO} and laminar flame profiles with D_T included in the transport property calculation. The profiles from laminar flames with non-unity and unity Le are also shown for comparison. The shadow area indicates the standard deviation.

which can be well assessed by turbulent diffusivity. The laminar flame results with unity Le also provide promising predictions of the mean turbulent flame structure, which is consistent with Refs. [36–38].

3.3. Effects of turbulence on the formation of NO

An important pollutant of ammonia combustion is NO. To understand the NO formation characteristics, the NO pathways in both the turbulent and laminar flames are analyzed, and the impact of turbulence on NO formation is also discussed in this subsection.

The global nitrogen flows of the laminar flames are shown in Fig. 11. The diagrams are based on the chemical mechanism as described in Sec. 2. It is first noted that NH_3 is consumed and converted to NH_2, and NH_2 is attacked by radicals such as H, O and OH to produce HNO, NH, NNH and N_2, of which NH is the main product of NH_2. NH is further converted to HNO, NO, N, N_2O,

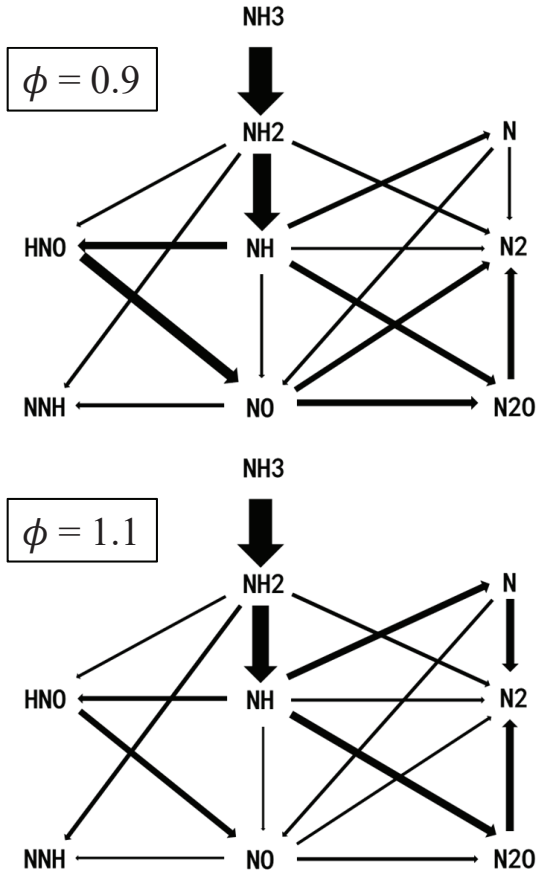

Figure 11: The global nitrogen flow diagrams for the laminar flames. The thickness of the arrows indicates the fraction of the nitrogen flow.

and N_2. An obvious difference of the reaction pathways between the lean and rich cases is that more NH is converted to HNO compared to N and N_2O in the lean case than that in the rich case, which further influences NO formation. To investigate the NO formation characteristics, six NO pathways, *i.e.* HNO, NH, N_2O, N_2, NNH and Zeldovich (thermal) [75] pathways, are defined based on the diagrams as shown in Table 2, where the main elementary reactions of various NO pathways are listed. The statistics of NO pathways for the turbulent and laminar flames are presented in the following.

Table 2: Elementary reactions in NO pathway

	Reaction	Pathway
R64:	$O_2 + HNO = NO + HO_2$	HNO
R83:	$HNO = NO + H$	HNO
R94:	$O + HNO = NO + OH$	HNO
R95:	$OH + HNO = NO + H_2O$	HNO
R96:	$H + HNO = NO + OH$	HNO
R44:	$O + NH = NO + H$	NH
R48:	$O_2 + NH = NO + OH$	NH
R51:	$N_2O + H = NO + NH$	N_2O
R39:	$H_2O + N_2 = NO + NH2$	N_2
R52:	$OH + N_2 = NO + NH$	N_2
R40:	$OH + NNH = NO + NH2$	NNH
R71:	$O + NNH = NO + NH$	NNH
R80:	$O + N_2 = NO + N$	Zeldovich
R101:	$O_2 + N = NO + O$	Zeldovich
R102:	$OH + N = NO + H$	Zeldovich

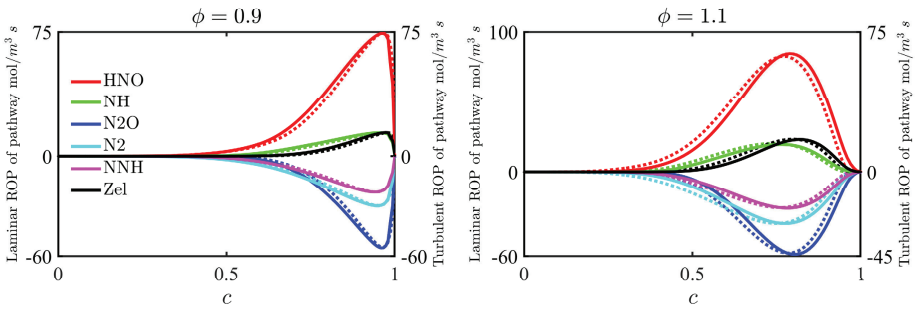

Figure 12: The conditional means of the rates of production (ROP) of various NO pathways for the lean and rich cases. The solid line and dotted line denotes the turbulent and corresponding laminar results respectively.

Figure 12 shows the conditional means of the rates of production (ROP) of various NO pathways for the lean and rich cases in c space. ROP in each pathway is the sum of NO reaction rate of all the elementary reactions involved in that pathway. Positive and negative ROP represents NO production and consumption, respectively. It is observed that the HNO pathway and N_2O pathway play the most important role in the formation and consumption of NO, respectively, which is consistent with previous studies [76–78]. For the lean case, the magnitude of NO pathways is very close between the laminar and

turbulent flames. For the rich case, however, the magnitude of NO pathways is lower than that of the laminar flame. An important observation is that the relative contributions from various NO pathways remain unchanged between the turbulent and laminar flames for both the lean and rich cases.

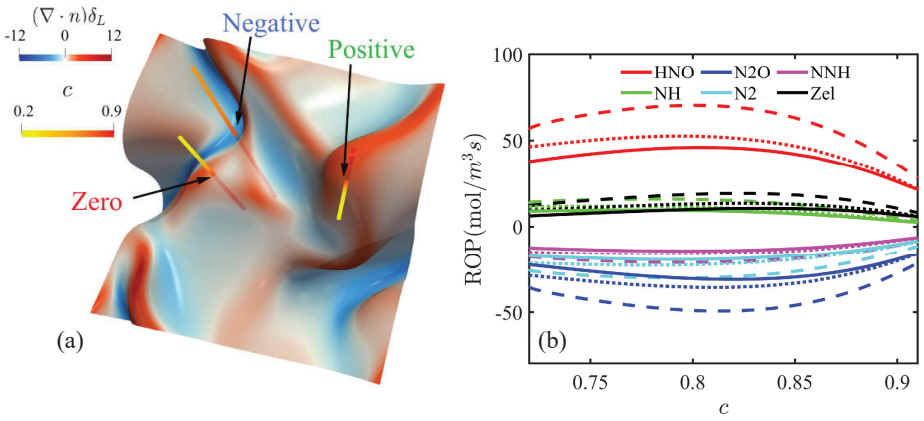

Figure 13: (a) Schematic diagram of the flame surface colored by curvature for the rich case. Three lines vertically across the flame surface with positive, negative and zero curvatures. (b) The profiles of various NO pathways along the three lines as a function of c near the reaction zone. (Positive : '—'; negative: '- - -'; and zero : '...' .)

It is noted that in Fig. 4 that the mass fraction of NO is higher in negative curvature regions than that in positive curvature regions in the rich case. It is interesting to examine the NO pathways in regions with different curvatures. Fig. 13a shows the flame front colored by the value of curvature for the rich case. It is seen that the flame front is highly wrinkled, and both large positive and negative curvature regions are observed. Three representative lines that are normal to the flame front are illustrated, which correspond to the flame locations with positive, zero and negative curvatures, respectively. Fig. 13b shows the profiles of various NO pathways along the three lines as a function of c near the reaction zone. It is interesting to see that, the magnitude of NO pathways is the highest in negatively curved regions, and the lowest in the region with positive curvature, consistent with the distribution of the NO mass fraction

in Fig. 4. It is also noted that the relative importance of various NO pathways rarely changes with curvature. From the above analysis, it is concluded that turbulence has evident impacts on the magnitude of NO pathways both globally and locally. However, the relative contributions of various NO pathways are not sensitive to the flow conditions.

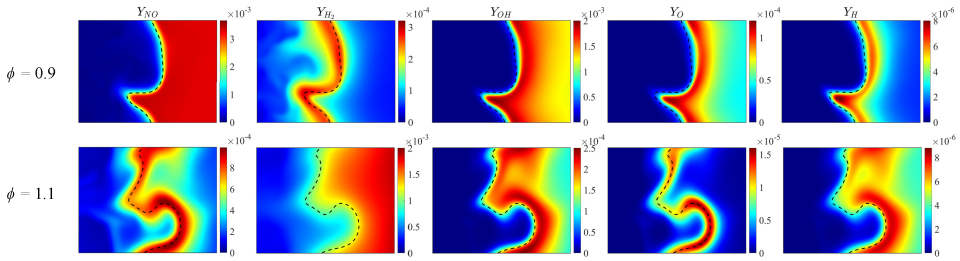

Figure 14: Contours of Y_{NO}, $Y_{\mathrm{H_2}}$, Y_{OH}, Y_{O} and Y_{H} near the flame front in a typical $x-y$ plane. The black dashed line indicates the flame front.

Next, more analyses are performed to further understand the effects of curvature on the NO formation. Fig. 14 shows the contours of Y_{NO}, $Y_{\mathrm{H_2}}$, Y_{OH}, Y_{O} and Y_{H} near the flame front in a typical $x-y$ plane. It is noted that, in the rich case, the mass fractions of NO and other radicals are larger in negative curvature regions than those in the positive curvature regions. In contrast, the distribution of NO mass fraction in the lean case does not show obvious correlation with curvature. The negative correlations between Y_{NO} and curvature in the rich case are further explained in the following.

Figure 15 shows the contour of the mass fraction of $\mathrm{H_2}$ with a schematic of the local curvature effects on species diffusion for the rich case. As can be seen, $\mathrm{H_2}$ diffuses from the product side to the reactant side, and is concentrated in negative curvature regions while its concentration is lower in positive curvature regions. Fig. 16a shows the JPDF of the $\mathrm{H_2}$ mass fraction and c. It is seen that $\mathrm{H_2}$ mass fraction increases monotonically in the progress variable space, which explains the diffusion of the $\mathrm{H_2}$ from the product side to the reactant

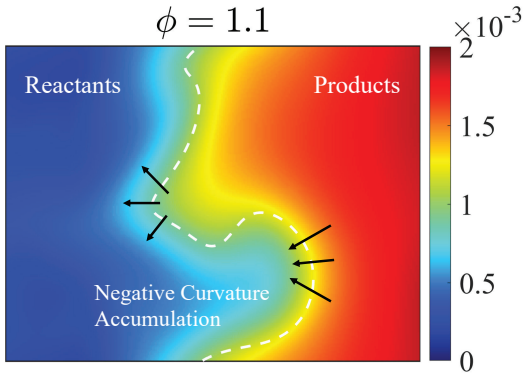

Figure 15: Contours of H_2 mass fraction with a schematic of the local curvature effects of lean and rich cases. The white dashed line indicates the flame front. The arrows denote the directions of H_2 diffusion.

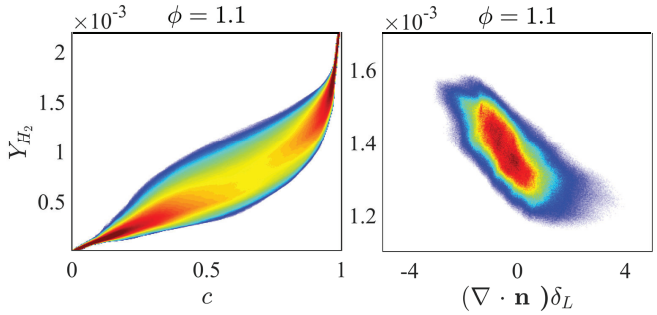

Figure 16: (a) JPDF of Y_{H_2} and progress variable. (b) JPDF of Y_{H_2} and curvature conditioned on the flame front.

side. Fig. 16b displays the JPDF of the H_2 mass fraction and curvature conditioned on the flame front. Again, a negative correlation between the H_2 mass fraction and curvature is found, showing that the H_2 mass fraction is higher in negative curvature regions. The correlations between the radical concentration and curvature are also observed in the Fig. 14. The negative correlation between the NO concentration/reaction and curvature is, therefore, related to the preferential diffusion effects of important radicals in the NO pathways (see Table 2). This scenario is different from those for flames with hydrogen or hydrogen-blended fuels [19, 79], where H_2 preferentially diffuses into positive

curvature regions.

In summary, turbulence rarely affects the relative contributions of nitrogen pathways. Instead, it influences the magnitude of pathways. The NO mass fraction and reaction rate are negatively correlated with curvature. The reactions in negative curvature regions are enhanced by the accumulations of radicals such as H_2 due to the preferential diffusion effects in turbulent flames.

4. Conclusions

In this study, three-dimensional direct numerical simulation of ammonia/air turbulent flames with two equivalence ratios of 0.9 and 1.1 were performed. The effects of turbulence on the flame structures were examined. The NO pathways were analyzed and the role of preferential diffusion of the radicals on NO formation was reported. The main findings are summarized as follows:

- The general flame characteristics were examined. It is found that NO is high in the product of the lean case and is high in the reaction zone of the rich, while H_2 is high in the reaction zone of the lean case and is high in the product of the rich case due to the pyrolization of NH_3. The conditional means of the species mass fractions and HRR from the DNS were compared with the profiles from laminar flames with varying strain rates. The effects of turbulence on the distributions of the species were investigated by analyzing the species transport equation. It was found that turbulent diffusion plays an important role in species transport in different regions of the turbulent flame.

- Turbulent mixing in the turbulent flame was quantified using the turbulent diffusivity D_T. Laminar premixed flames with various diffusivities were simulated and the results were compared with those of the DNS. It was showed that the conditional means of the DNS agree well with the profiles

of the laminar premixed flame with D_T both in the lean and rich cases. The influence of turbulence on flame structure is to increase the thermal and species diffusion, which can be well assessed by turbulent diffusivity.

- The global and local effects of turbulence on the formation of NO were studied. The NO pathways are compared between the turbulent and laminar flames for the lean and rich flames. The local NO pathways from three representative regions with positive, zero and negative curvatures were examined, and it was concluded that turbulence has evident impacts on the magnitude of NO pathways both globally and locally. However, the relative contributions of various NO pathways are not sensitive to the flow conditions. The negative correlations between Y_{NO} and curvature were observed for the rich case. It was suggested that the magnitude of various NO pathways is enhanced in negative curvature regions due to the accumulations of radicals such as H_2 related to the preferential diffusion effects in turbulent flames.

Acknowledgments

This work was supported by Natural Science Foundation of China (Grant Nos.: 52022091, 51976185, 91841302). The work was also supported by the Fundamental Research Funds for the Central Universities.

References

[1] J. A. Ritter, A. D. Ebner, J. Wang, R. Zidan, Implementing a hydrogen economy, Mater. Today 6 (2003) 18–23.

[2] C. Brackmann, B. Zhou, Z. S. Li, M. Aldén, Strategies for Quantitative Planar Laser-Induced Fluorescence of NH Radicals in Flames, Combust. Sci. Technol. 188 (2016) 529–541.

[3] C. Brackmann, B. Zhou, P. Samuelsson, V. A. Alekseev, A. A. Konnov, Z. Li, Marcus Aldén, Strategy for improved NH2 detection in combustion environments using an Alexandrite laser, Spectrochim. Asta A 184 (2017) 235–242.

[4] W. Weng, C. Brackmann, M. Aldén, Z. Li, Planar laser-induced photofragmentation fluorescence for quantitative ammonia imaging in combustion environments, Combust. Flame (2021) 111687.

[5] A. Hayakawa, Y. Arakawa, R. Mimoto, K. K. A. Somarathne, T. Kudo, H. Kobayashi, Experimental investigation of stabilization and emission characteristics of ammonia/air premixed flames in a swirl combustor, Int. J. Hydrog. Energy 42 (19) (2017) 14010–14018.

[6] A. Ichikawa, Y. Naito, A. Hayakawa, T. Kudo, H. Kobayashi, Burning velocity and flame structure of CH4/NH3/air turbulent premixed flames at high pressure, Int. J. Hydrog. Energy 44 (13) (2019) 6991–6999.

[7] E. C. Okafor, K. K. A. Somarathne, A. Hayakawa, T. Kudo, O. Kurata, N. Iki, H. Kobayashi, Towards the development of an efficient low-nox ammonia combustor for a micro gas turbine, Proc. Combust. Inst. 37 (4) (2019) 4597–4606.

[8] Q. Fan, X. Liu, L. Xu, A. A. Subash, C. Brackmann, M. Aldén, X.-S. Bai, Z. Li, Flame structure and burning velocity of ammonia/air turbulent premixed flames at high karlovitz number conditions, Combust. Flame 238 (2022) 111943.

[9] Q. Fan, X. Liu, X. Cai, C. Brackmann, M. Alden, X.-S. Bai, Z. Li, Structure and scalar correlation of ammonia/air turbulent premixed flames in the distributed reaction zone regime, Combust. Flame 241 (2022) 112090.

[10] M. Zhang, X. Wei, J. Wang, Z. Huang, H. Tan, The blow-off and transient characteristics of co-firing ammonia/methane fuels in a swirl combustor, Proc. Combust. Inst. 38 (4) (2021) 5181–5190.

[11] S. Zhou, W. Yang, H. Tan, Q. An, J. Wang, H. Dai, X. Wang, X. Wang, S. Deng, Experimental and kinetic modeling study on NH3/syngas/air and NH3/bio-syngas/air premixed laminar flames at elevated temperature, Combust. Flame 233 (2021) 111594.

[12] L. Ji, J. Wang, G. Hu, R. Mao, W. Zhang, Z. Huang, Experimental study on structure and blow-off characteristics of NH3/CH4 co-firing flames in a swirl combustor, Fuel 314 (2022) 123027.

[13] X. Wei, M. Zhang, Z. An, J. Wang, Z. Huang, H. Tan, Large eddy simulation on flame topologies and the blow-off characteristics of ammonia/air flame in a model gas turbine combustor, Fuel 298 (2021) 120846.

[14] E. C. Okafor, K. A. Somarathne, R. Ratthanan, A. Hayakawa, T. Kudo, O. Kurata, N. Iki, T. Tsujimura, H. Furutani, H. Kobayashi, Control of nox and other emissions in micro gas turbine combustors fuelled with mixtures of methane and ammonia, Combust. Flame 211 (2020) 406–416.

[15] K. D. K. A. Somarathne, S. Hatakeyama, A. Hayakawa, H. Kobayashi, Numerical study of a low emission gas turbine like combustor for turbulent ammonia/air premixed swirl flames with a secondary air injection at high pressure, Int. J. Hydrog. Energy 42 (44) (2017) 27388–27399.

[16] S. Wiseman, M. Rieth, A. Gruber, J. R. Dawson, J. H. Chen, A comparison of the blow-out behavior of turbulent premixed ammonia/hydrogen/nitrogen-air and methane–air flames, Proc. Combust. Inst. 38 (2021) 2869–2876.

[17] K. D. K. Somarathne, A. Hayakawa, H. Kobayashi, Numerical investigation on the combustion characteristics of turbulent premixed ammonia/air flames stabilized by a swirl burner, J. Fluid Sci. Technol. 11 (2016) 0026–0026.

[18] R. Khamedov, W. Song, F. E. H. Perez, H. G. Im, A Computational Study of Ammonia Combustion in MILD Conditions, AIAA Scitech 2021 Forum.

[19] C. Netzer, A. Ahmed, A. Gruber, T. Lovas, Curvature effects on NO formation in wrinkled laminar ammonia/hydrogen/nitrogen-air premixed flames, Combust. Flame 232 (2021) 111520.

[20] M. Rieth, A. Gruber, F. A. Williams, J. H. Chen, Enhanced burning rates in hydrogen-enriched turbulent premixed flames by diffusion of molecular and atomic hydrogen, Combust. Flame (2021) 111740.

[21] W. Yang, K. Ranga Dinesh, K. Luo, D. Thevenin, Direct numerical simulation of turbulent premixed ammonia and ammonia-hydrogen combustion under engine-relevant conditions, Int. J. Hydrog. Energy 47 (20) (2022) 11083–11100.

[22] H. Wang, E. R. Hawkes, J. H. Chen, A direct numerical simulation study of flame structure and stabilization of an experimental high Ka CH4/air premixed jet flame, Combust. Flame 180 (2017) 110–123.

[23] H. Wang, E. R. Hawkes, J. H. Chen, Turbulence-flame interactions in DNS of a laboratory high Karlovitz premixed turbulent jet flame, Phys. Fluids 28 (2016) 095107.

[24] K. Ranga Dinesh, H. Shalaby, K. Luo, J. van Oijen, D. Thévenin, High hydrogen content syngas fuel burning in lean premixed spherical flames at

elevated pressures: Effects of preferential diffusion, Int. J. Hydrog. Energy 41 (40) (2016) 18231–18249.

[25] K. Ranga Dinesh, H. Shalaby, K. Luo, J. van Oijen, D. Thévenin, Heat release rate variations in high hydrogen content premixed syngas flames at elevated pressures: Effect of equivalence ratio, Int. J. Hydrog. Energy 42 (10) (2017) 7029–7044.

[26] P. A. Libby, F. A. Williams, Strained premixed laminar flames under nonadiabatic conditions, Combust. Sci. Technol. 31 (1-2) (1983) 1–42.

[27] N. Darabiha, S. Candel, F. Marble, The effect of strain rate on a premixed laminar flame, Combust. Flame 64 (2) (1986) 203–217.

[28] B. Rogg, Response and flamelet structure of stretched premixed methane/air flames, Combust. Flame 73 (1) (1988) 45–65.

[29] F. N. Egolfopoulos, Dynamics and structure of unsteady, strained, laminar premixed flames, Symp. (Int.) Combust. 25 (1) (1994) 1365–1373.

[30] T. Echekki, J. H. Chen, Unsteady strain rate and curvature effects in turbulent premixed methane-air flames, Combust. Flame 106 (1) (1996) 184–202.

[31] E. R. Hawkes, J. H. Chen, Comparison of direct numerical simulation of lean premixed methane–air flames with strained laminar flame calculations, Combust. Flame 144 (1) (2006) 112–125.

[32] A. N. Lipatnikov, T. Nilsson, R. Yu, X. S. Bai, V. A. Sabelnikov, Assessment of a flamelet approach to evaluating mean species mass fractions in moderately and highly turbulent premixed flames, Phys. Fluids 33 (4) (2021) 045121.

[33] N. Peters, Turbulent Combustion, Cambridge University Press, 2001.

[34] A. Lipatnikov, J. Chomiak, Effects of premixed flames on turbulence and turbulent scalar transport, Prog. Energy Combust. Sci. 36 (1) (2010) 1–102.

[35] T. Elperin, N. Kleeorin, M. Liberman, A. N. Lipatnikov, I. Rogachevskii, R. Yu, Turbulent diffusion of chemically reacting flows: Theory and numerical simulations, Phys. Rev. E 96 (2017) 053111.

[36] B. Savard, G. Blanquart, An a priori model for the effective species lewis numbers in premixed turbulent flames, Combust. Flame 161 (6) (2014) 1547–1557.

[37] A. Aspden, M. Day, J. Bell, Three-dimensional direct numerical simulation of turbulent lean premixed methane combustion with detailed kinetics, Combust. Flame 166 (2016) 266–283.

[38] B. Savard, B. Bobbitt, G. Blanquart, Structure of a high Karlovitz n-C7H16 premixed turbulent flame, Proc. Combust. Inst. 35 (2015) 1377–1384.

[39] A. J. Aspden, M. S. Day, J. B. Bell, Towards the distributed burning regime in turbulent premixed flames, J. Fluid Mech. 871 (2019) 1–21.

[40] R. C. Rocha, M. Costa, X.-S. Bai, Combustion and emission characteristics of ammonia under conditions relevant to modern gas turbines, Combust. Sci. Technol. 193 (14) (2021) 2514–2533.

[41] R. C. Rocha, S. Zhong, L. Xu, X.-S. Bai, M. Costa, X. Cai, H. Kim, C. Brackmann, Z. Li, M. Aldén, Structure and laminar flame speed of an ammonia/methane/air premixed flame under varying pressure and equivalence ratio, Energy Fuels 35 (9) (2021) 7179–7192.

[42] T. Tomidokoro, T. Yokomori, H. G. Im, Numerical study on propagation and NO reduction behavior of laminar stratified ammonia/air flames, Combust. Flame 241 (2022) 112102.

[43] M. Zhang, Z. An, X. Wei, J. Wang, Z. Huang, H. Tan, Emission analysis of the CH4/NH3/air co-firing fuels in a model combustor, Fuel 291 (2021) 120135.

[44] M. Zhang, Z. An, L. Wang, X. Wei, B. Jianayihan, J. Wang, Z. Huang, H. Tan, The regulation effect of methane and hydrogen on the emission characteristics of ammonia/air combustion in a model combustor, Int. J. Hydrog. Energy 46 (40) (2021) 21013–21025.

[45] Z. An, M. Zhang, W. Zhang, R. Mao, X. Wei, J. Wang, Z. Huang, H. Tan, Emission prediction and analysis on CH4/NH3/air swirl flames with LES-FGM method, Fuel 304 (2021) 121370.

[46] T. Honzawa, R. Kai, A. Okada, A. Valera-Medina, P. J. Bowen, R. Kurose, Predictions of NO and CO emissions in ammonia/methane/air combustion by LES using a non-adiabatic flamelet generated manifold, Energy 186 (2019) 115771.

[47] D. Dasgupta, W. Sun, M. Day, A. J. Aspden, T. Lieuwen, Analysis of chemical pathways and flame structure for n-dodecane/air turbulent premixed flames, Combust. Flame 207 (2019) 36–50.

[48] C. Jiménez, B. Cuenot, T. Poinsot, D. Haworth, Numerical simulation and modeling for lean stratified propane-air flames, Combust. Flame 128 (1) (2002) 1–21.

[49] P. Trisjono, H. Pitsch, A direct numerical simulation study on no formation in lean premixed flames, Proc. Combust. Inst. 36 (2) (2017) 2033–2043.

[50] M. S. Day, J. B. Bell, X. Gao, P. Glarborg, Numerical simulation of nitrogen oxide formation in lean premixed turbulent H2/O2/N2 flames, Proc. Combust. Inst. 33 (1) (2011) 1591–1599.

[51] J. Bell, M. Day, M. Lijewski, Simulation of nitrogen emissions in a premixed hydrogen flame stabilized on a low swirl burner, Proc. Combust. Inst. 34 (1) (2013) 1173–1182.

[52] O. Mathieu, E. L. Petersen, Experimental and modeling study on the high-temperature oxidation of Ammonia and related NOx chemistry, Combust. Flame 162 (2015) 554–570.

[53] M. Cheng, H. Wang, H. Xiao, K. Luo, J. Fan, Emission characteristics and heat release rate surrogates for ammonia premixed laminar flames, Int. J. Hydrog. Energy 46 (2021) 13461–13470.

[54] P. L. Carroll, G. Blanquart, A proposed modification to Lundgren's physical space velocity forcing method for isotropic turbulence, Phys. Fluids 25 (2013) 105114.

[55] P. E. Hamlington, A. Y. Poludnenko, E. S. Oran, Interactions between turbulence and flames in premixed reacting flows, Phys. Fluids 23 (12) (2011) 125111.

[56] B. Bobbitt, S. Lapointe, G. Blanquart, Vorticity transformation in high karlovitz number premixed flames, Phys. Fluids 28 (1) (2016) 015101.

[57] A. Kazbekov, A. M. Steinberg, Flame- and flow-conditioned vorticity transport in premixed swirl combustion, Proc. Combust. Inst. 38 (2) (2021) 2949–2956.

[58] W. S. Chai, Y. Bao, P. Jin, G. Tang, L. Zhou, A review on ammonia, ammonia-hydrogen and ammonia-methane fuels, Renew. Sust. Energ. Rev. 147 (2021) 111254.

[59] T. Lu, C. K. Law, A directed relation graph method for mechanism reduction, Proc. Combust. Inst. 30 (2005) 1333–1341.

[60] C. S. Yoo, H. G. Im, Characteristic boundary conditions for simulations of compressible reacting flows with multi-dimensional, viscous and reaction effects, Combust. Theory Model. 11 (2007) 259–286.

[61] J. H. Chen, A. Choudhary, B. de Supinski, M. DeVries, E. R. Hawkes, S. Klasky, W. K. Liao, K. L. Ma, J. Mellor-Crummey, N. Podhorszki, R. Sankaran, S. Shende, C. S. Yoo, Terascale direct numerical simulations of turbulent combustion using S3D, Comput. Sci. Disc. 2 (2009) 015001.

[62] H. Wang, E. R. Hawkes, B. Zhou, J. H. Chen, Z. Li, M. Aldén, A comparison between direct numerical simulation and experiment of the turbulent burning velocity-related statistics in a turbulent methane-air premixed jet flame at high Karlovitz number, Proc. Combust. Inst. 36 (2017) 2045–2053.

[63] H. Wang, E. R. Hawkes, J. H. Chen, Direct numerical simulations of a high Karlovitz number laboratory premixed jet flame - An analysis of flame stretch and flame thickening, J. Fluid Mech. 815 (2017) 511–536.

[64] C. A. Kennedy, M. H. Carpenter, Several new numerical methods for compressible shear-layer simulations, Appl. Numer. Math. 14 (1994) 397–433.

[65] J. F. Driscoll, Turbulent premixed combustion: Flamelet structure and its effect on turbulent burning velocities, Prog. Energy Combust. Sci. 34 (1) (2008) 91–134.

[66] A. Aspden, M. Day, J. Bell, Turbulence–flame interactions in lean premixed hydrogen: transition to the distributed burning regime, J. Fluid Mech. 680 (2011) 287–320.

[67] A. Aspden, A numerical study of diffusive effects in turbulent lean premixed hydrogen flames, Proc. Combust. Inst. 36 (2) (2017) 1997–2004.

[68] A. Aspden, J. Bell, M. Day, F. Egolfopoulos, Turbulence–flame interactions in lean premixed dodecane flames, Proc. Combust. Inst. 36 (2) (2017) 2005–2016.

[69] J. You, Y. Yang, Modelling of the turbulent burning velocity based on lagrangian statistics of propagating surfaces, J. Fluid Mech. 887 (2020) A11.

[70] Z. Lu, Y. Yang, Modeling pressure effects on the turbulent burning velocity for lean hydrogen/air premixed combustion, Proc. Combust. Inst. 38 (2) (2021) 2901–2908.

[71] N. Peters, Laminar flamelet concepts in turbulent combustion, Symp. (Int.) Combust. 21 (1) (1988) 1231–1250.

[72] T. Poinsot, D. Veynante, Theoretical and Numerical Combustion, RT Edwards, Inc., 2005.

[73] D. Veynante, A. Trouvé, K. N. C. Bray, T. Mantel, Gradient and counter-gradient scalar transport in turbulent premixed flames, J. Fluid Mech. 332 (1997) 263–293.

[74] H. Tennekes, J. L. Lumley, A first course in turbulence, MIT press, 1972.

[75] Y. B. Zeldovich, The oxidation of nitrogen in combustion and explosions, Acta Physicochim. 21 (1946) 557–626.

[76] J. A. Miller, M. D. Smooke, R. M. Green, R. J. Kee, Kinetic modeling of the oxidation of ammonia in flames, Combust. Sci. Technol. 34 (1-6) (1983) 149–176.

[77] C. Duynslaegher, F. Contino, J. Vandooren, H. Jeanmart, Modeling of ammonia combustion at low pressure, Combust. Flame 159 (9) (2012) 2799–2805.

[78] K. P. Shrestha, L. Seidel, T. Zeuch, F. Mauss, Detailed kinetic mechanism for the oxidation of ammonia including the formation and reduction of nitrogen oxides, Energy Fuels 32 (10) (2018) 10202–10217.

[79] A. Aspden, M. Day, J. Bell, Characterization of low Lewis number flames, Proc. Combust. Inst. 33 (2011) 1463–1471.